The Influence of Structure on the Electrochemical and Thermal Response of Li-Ion Battery Electrodes

Prehit Patel
Department of Mechanical and Aerospace Engineering,
University of Alabama in Huntsville,
301 Sparkman Drive,
Huntsville, AL 35899
e-mail: ppp0002@uah.edu

George J. Nelson
Department of Mechanical and Aerospace Engineering,
University of Alabama in Huntsville,
301 Sparkman Drive,
Huntsville, AL 35899
e-mail: George.Nelson@uah.edu

Advancement of lithium-ion batteries for transportation applications requires addressing two key challenges: increasing energy density and providing fast charging capabilities. The first of these challenges can be met using thicker electrodes. However, the implementation of thick electrodes inherently presents a trade-off with respect to fast charging. As the thickness is increased, transport limitations reduce the ability of the battery to meet aggressive charge conditions. At the particle scale, interactions between solid diffusion and reaction kinetics influence the effective storage of lithium. At the electrode scale, diffusion limitations can lead to local variations in salt concentrations and electric potential. These short-range and long-range effects can combine to influence local current and heat generation. In the present work, a pseudo-2D lithium-ion battery model is applied to understand how active material particle size, porosity, and electrode thickness impact local field variables, current, heat generation, and cell capacity within a single-cell stack. The model was built assuming that the active particles are representative spherical particles. The governing equations and boundary conditions were set following the common Newman model. Cell response under varied combinations of charge and discharge cycling is assessed for rates of 1 C and 5 C. Aggressive charge and discharge conditions lead to locally elevated C-rates and attendant increases in local heat generation. These variations can be impacted in part by tailoring electrode structures. To this end, results for parametric studies of active material particle size, porosity, and electrode thickness are presented and discussed. [DOI: 10.1115/1.4045820]

Keywords: energy storage systems, lithium-ion batteries, fast charge, thick electrodes, thermal management

1 Introduction

One key global challenge is to meet the increasing energy demand using sustainable energy sources which can help mitigate CO_2 emissions and climate change. Increased vehicle fleet electrification, supported by renewable electricity, is one tool that can be applied to achieve this goal. Energy storage is a critical component for fleet electrification and grid integration of renewable energy. Lithium-ion (Li-ion) batteries are known for their high energy density, high current density, and low self-discharge. Due to the reasons mentioned above lithium-ion batteries have become the primary energy storage technology for electric and hybrid vehicles [1–5].

The continued advancement of lithium-ion batteries for transportation applications requires addressing two key challenges: increasing energy density and providing fast charging capabilities. The first of these challenges can be met in part through the use of thicker electrodes, which reduce the electrochemically inactive mass of the cell. Singh et al. showed that thicker electrodes provide higher energy density compared with thinner electrodes [6]. However, the implementation of thick electrodes inherently presents a trade-off with respect to fast charging capabilities. As the thickness is increased, transport limitations exert a greater influence on battery performance and reduce the ability of the battery to meet aggressive charge conditions. Zhao et al. performed various studies on the electrochemical and thermal behavior of thick electrodes for Li-ion batteries [7]. Their results show that thicker electrodes can store more active material and thus provide higher energy density. However, thicker electrodes show uneven heating throughout the cell compared with thin electrodes. This uneven heat distribution throughout the cell can lead to the degradation of active material which eventually decreases the realized cell capacity. While performing fast charge and discharge in thick electrodes, there is a loss of realized capacity due to longer diffusion paths, which limit access to active material. Also, at higher C-rates in thick electrodes, there is a risk of lithium plating during charging. Lithium plating occurs when electrochemical conditions in the anode favor the deposition of metallic lithium, instead of intercalation into the active material. Lithium plating can occur on the anode while charging at high C-rates or low temperatures. Lithium plating can affect battery life and safety [8,9]. Most notably lithium plating can lead to dendrite growth and internal short circuits.

At the particle scale, interactions between solid diffusion and reaction kinetics influence the effective storage of lithium within the active material. At the electrode scale, diffusion limitations can lead to local variations in salt concentrations and electric potential. These short-range and long-range effects can combine to influence local current and heat generation in thick and thin electrodes [10]. The battery performance is also influenced by various parameters like porosity, particle size, and tortuosity. The analysis of Taleghani et al. showed that there is an optimal porosity value. Below and beyond this optimal value, the realized capacity of the cell decreases due to kinetic and mass transfer limitations [11]. Taleghani et al. also performed studies on the effect of particle size distributions on cell performance. Stein et al. performed various studies on how particle size affects the cell performance [12] and showed that the planetary ball milling of electrode materials resulted in smaller crystallite size. However, the benefits of the

Contributed by the Advanced Energy Systems Division of ASME for publication in the Journal of Energy Resources Technology. Manuscript received September 2, 2019; final manuscript received December 6, 2019; published online December 20, 2019. Assoc. Editor: Navid Goudarzi.

size reduction were found to be limited in some cases, with intermediate crystallite sizes showing better overall performance due to reduced agglomeration and lower interfacial resistance. Tran et al. investigated how the particle size influences the discharge behavior and capacity of the lithium-ion graphite electrode [13] and reported that graphite electrodes with 6 μm diameter particle size at C/2 discharge rate was 80% of that at a C/24 rate, whereas the capacity of electrodes with particles of 44 μm size at a discharge rate of C/2 was estimated at 25% of the capacity obtained a C/24 rate.

Lithium-ion batteries have wide applications including performing fast charge/discharge and operating under a wide range of temperatures. The thermal stability of the battery is necessary for safe and reliable operation. Considering that, it is very important to understand the thermal behavior in lithium-ion batteries. A thorough critical review on the thermal behavior of lithium-ion batteries was provided by Bandhauer et al. Experimental approaches and numerical models of electrodes of varied thicknesses made from different materials were assessed to understand their thermal effects on the battery performance [14]. Fast charging and discharging of thick electrodes contribute to heat generation inside the battery which can also affect battery life and capacity. The cell power and capacity can be significantly dropped when operating them at temperatures above 50 °C. It also shows that performing charge and discharge processes below 10 °C increase the risk of lithium plating. Thomas et al. performed a wide range of experiments from 25 °C to 60 °C and 60% to 100% state of charge (SOC) to understand the power degradation in lithium-ion batteries [15]. Their results showed that the elevated temperature can cause capacity and power degradation in the battery. The result also showed that for 60–80% SOC the degradation of the cells is driven by temperature.

The continued advancement of the lithium-ion battery is necessary to fulfill the energy storage needs of more sustainable energy infrastructure. Application of thick electrodes can improve the energy density. Lithium-ion batteries incorporating thick electrodes could be readily used in stationary energy storage applications that experience lower C-rate charge and discharge. Such electrodes perform well at lower C-rates compared to fast charging and discharging. However, to meet the demand for electric transportation, the lithium-ion battery must provide higher energy density combined with faster-charging capabilities. As noted, the use of thick electrodes creates a critical trade-offs with fast charging demands. This trade-off occurs because as thickness increases internal transport resistance increases, which can have an adverse effect on battery performance and reduce the ability to meet aggressive charge conditions. Fast charging can also have adverse effects like lithium plating and excess heat generation. It has been shown that the performance of thick electrodes can be enhanced by increasing the porosity and decreasing the tortuosity of the electrodes [16]. Other parameters related to electrode structure and particle size can influence battery performance [12,13].

In this paper, a detailed study of lithium-ion battery performance using a pseudo-2D (P2D) model is presented. Initially, the model was validated against the experimental results obtained from Stein et al. [12]. The P2D model was used to understand how various parameters like porosity, particle size, and electrode thickness affect battery performance. Thin and thick electrodes were simulated during discharge at 1 C and charge at 1 C and 5 C. Local field variables like surface solid lithium concentration and electrolyte salt concentration along with responses including local current generation were analyzed for 1 C discharge and an aggressive 5 C charge. Reversible and irreversible heat generation for thin and thick electrodes for distinct combinations of particle sizes were also analyzed at 1 C discharge and 5 C charge rate. The study indicates that an increase in porosity can increase realized cell capacity. Conversely, an increase in particle size decreases realized cell capacity. Total heat generation in thick electrodes is higher compared with that in the thin electrode. Thick electrodes also show more localized variation in current density and heat generation compared with thin electrodes, which may accelerate the degradation of active material. The results presented reveal a need for design at both microstructural and cell levels to accommodate fast charging in more energy-dense lithium-ion batteries.

2 Model Description

In the present work, COMSOL MULTIPHYSICS 5.2 software is used to fully develop a P2D model of lithium-ion battery. The P2D COMSOL model is based on the governing equations and boundary conditions of the Newman model [17]. The lithium-ion battery geometry definition and mesh generation were done in COMSOL. In this model Graphite (Li_xC_6) was used as a negative electrode active material and $Li(Ni_{1/3}Mn_{1/3}Co_{1/3})O_2$ (NMC) was used as a positive electrode active material. The electrolyte was taken to be lithium hexafluorophosphate ($LiPF_6$) in 1:1 ethylene carbonate and diethylene carbonate. Figure 1 illustrates the 1D model geometry developed in COMSOL MULTIPHYSICS 5.2 software. The mesh was generated using user-controlled mesh in COMSOL. To understand the lithium-ion battery performance, the time-dependent model was used. Initially, the battery was fully charged and then it was discharged at 1 C followed by an aggressive charging at 5 C. Physical parameters were obtained from the study by Guo et al. [18] and Gu and Wang [19], and the COMSOL Material Library. Geometrical parameters were obtained from the study by Stein et al. [12]. The physical and geometrical parameters used in the model are given in Table 1. The parameters for this study were chosen based on the experimental and simulation work presented in Refs. [12,18,19]. For the model validation, the COMSOL model parameters were matched with those of Stein et al. [12].

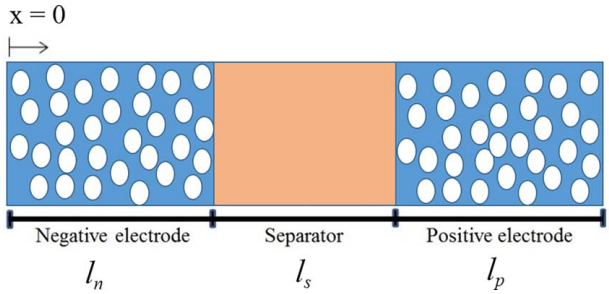

Fig. 1 Schematic of a P2D lithium-ion battery model

Table 1 List of model parameters [12,18,19]

Parameter	Description	Value
D_{neg}	Solid-phase Li diffusivity (Li_xC_6)	3.9×10^{-14} m^2/s
D_{pos}	Solid-phase Li diffusivity (NMC)	1×10^{-13} m^2/s
$D_{electrolyte}$	Electrolyte diffusivity	7.5×10^{-11} m^2/s
r_{pos}	Active particle radius	5×10^{-6} m
r_{neg}	Active particle radius	5×10^{-6} m
σ_{neg}	Solid-phase conductivity (Li_xC_6)	100 S/cm
σ_{pos}	Solid-phase conductivity (NMC)	0.14 S/cm
C_{L0}	Initial electrolyte concentration	1000 mol/m^3
C_{smax_neg}	Maximum surface concentration	29,000 mol/m^3
C_{smax_pos}	Maximum surface concentration	31,833 mol/m^3
L_{pos1}	Thickness of cathode (thin electrode)	14×10^{-6} m
L_{neg1}	Thickness of anode (thin electrode)	15×10^{-6} m
L_{pos2}	Thickness of cathode (thick electrode)	200×10^{-6} m
L_{neg2}	Thickness of anode (thick electrode)	200×10^{-6} m
L_{sep}	Thickness of separator	26×10^{-6} m
ε	Porosity	0.444
ε_s	Active material volume fraction	0.456
τ_i	Tortuosity	1.150
α_c	Reaction rate coefficient	0.5
α_a	Reaction rate coefficient	0.5
C	C-rate	1 C, 5 C
t_+^0	Lithium transference number	0.363
T	Temperature	298 K

3 Mathematical Model

The model basically is divided into three sections: material balance, charge balance, and energy balance. All governing equations are solved in the x-direction, across the battery thickness, as the primary spatial dimension.

The active material particles were considered as spherical particles for defining the material balance. The mass balance for the Li^+ ions in an active solid particle is given by Fick's second law in spherical coordinates:

$$\frac{\partial c_{s,i}}{\partial t} = D_{s,i}\frac{1}{r^2}\frac{\partial}{\partial r}\left(r^2\frac{\partial c_{s,i}}{\partial r}\right) \tag{1}$$

Here r is the radius of the particle, $i=p$ for the positive electrode, and $i=n$ for the negative electrode. Boundary conditions for mass balance in a solid spherical particle are shown below. At the center of the particle, the flux is given by Eq. (2). The negative sign represents the flux moving outward of the particle.

$$r=0\,, \qquad -D_{s,i}\left(\frac{\partial c_{s,i}}{\partial r}\right)=0 \tag{2}$$

At the surface of the particle, the flux is given by Eq. (3). The flux moving out from the surface of the particle is equal to the lithium-ion consumed or produced during the electrochemical reaction

$$r=R_{s,i}, \qquad -D_{s,i}\left(\frac{\partial c_{s,i}}{\partial r}\right)=J_i \tag{3}$$

Here J is pore wall flux of lithium ions moving outward from the active particle. The mass balance for the electrolyte in the liquid state is given by the Eq. (4) below:

$$\varepsilon_i\frac{\partial c_i}{\partial t} = D_{eff,i}\frac{\partial^2 c_i}{\partial x^2} + (1-t_+^0)\,a_i\,J_i \tag{4}$$

Here i indicates either the separator, the positive electrode, or the negative electrode, depending on the domain, and a_i is the electrode surface area. Equation (5) was used to calculate the electrode surface area.

$$a_i = \frac{3}{R_{s,i}}(1-\varepsilon_i-\varepsilon_f) \tag{5}$$

At both ends of the cell, there is no flux so boundary conditions for both ends are given by equations below:

$$-D_{eff,p}\left(\frac{\partial c_p}{\partial x}\right)_{x=0}=0 \tag{6}$$

$$-D_{eff,p}\left(\frac{\partial c_p}{\partial x}\right)_{x=L_p+L_s+L_n}=0 \tag{7}$$

At the negative electrode–separator junction and the positive electrode–separator junction, the concentration of the electrolyte and the flux is continuous, as shown in Eqs. (8)–(11)

$$(C_p)_{x=L_p^+} = (C_s)_{x=L_p^-} \tag{8}$$

$$(C_s)_{x=(L_p+L_s)^-} = (C_n)_{x=(L_p+L_s)^+} \tag{9}$$

$$-D_{eff,p}\left(\frac{\partial c_p}{\partial x}\right)_{x=L_p^-} = -D_{eff,s}\left(\frac{\partial c_s}{\partial x}\right)_{x=L_p^+} \tag{10}$$

$$-D_{eff,s}\left(\frac{\partial c_s}{\partial x}\right)_{x=(L_p+L_s)^-} = -D_{eff,n}\left(\frac{\partial c_n}{\partial x}\right)_{x=(L_p+L_s)^-} \tag{11}$$

The effective diffusion coefficient of the liquid electrolyte that fills the pore phase is corrected by porosity and tortuosity given in Eq. (12)

$$D_{eff,i} = D_i\frac{\varepsilon_i}{\tau_i} \tag{12}$$

The charge balance in the solid phase is determined using Ohm's law

$$-\sigma_{eff,i}\,\frac{\partial^2\phi_{1,i}}{\partial x^2} = a_i\,F\,J_i \tag{13}$$

Here F is Faraday's constant, ϕ is the potential in the solid phase, and σ_{eff} is the effective conductivity. The effective conductivity is determined using the Eq. (14) below:

$$-\sigma_{eff,i} = \sigma_i\,(1-\varepsilon_i-\varepsilon_{f,i}) \tag{14}$$

The charge flux at the junction of the current collector and the positive electrode is equal to the current density applied to the cell initially

$$-\sigma_{eff,p}\left(\frac{\partial\phi_{1,p}}{\partial x}\right)_{x=0} = i_{app} \tag{15}$$

The boundary conditions at the junction of the negative electrode–separator and positive electrode–separator are given below:

$$-\sigma_{eff,p}\left(\frac{\partial\phi_{1,p}}{\partial x}\right)_{x=L_p}=0 \tag{16}$$

$$-\sigma_{eff,n}\left(\frac{\partial\phi_{1,n}}{\partial x}\right)_{x=L_p+L_s}=0 \tag{17}$$

The potential of solid phase at the negative electrode end of the cell was set to zero and the potential of the solid phase at the positive electrode end of the cell was set to cell voltage, i.e., 4.2 V. The charge balance for the electrolyte in the liquid phase is determined using Ohm's law in the following equation:

$$-\frac{\partial}{\partial x}\left(k_{eff,i}\frac{\partial\phi_{2,i}}{\partial x}\right) + \frac{2RT\,(1-t_+^0)}{F}\frac{\partial}{\partial x}\left(k_{eff,i}\frac{\partial lnc_i}{\partial x}\right) = a_iF\,J_i \tag{18}$$

Here k_{eff} is the specific conductivity of the binary electrolyte and i stands for separator, the positive electrode and the negative electrode. The specific conductivity k_{eff} can be calculated using Equation (19) below:

$$k_{eff,i} = k_i\frac{\varepsilon_i}{\tau_i} \tag{19}$$

At both the ends of the cell, there is no charge flux in the liquid phase so the boundary conditions for both the ends are given by the equations below:

$$-k_{eff,p}\left(\frac{\partial\phi_{2,p}}{\partial x}\right)_{x=0}=0 \tag{20}$$

$$-k_{eff,n}\left(\frac{\partial\phi_{2,n}}{\partial x}\right)_{x=L_p+L_s+L_n}=0 \tag{21}$$

The pore wall flux J_i can be obtained using Bulter–Volmer in Eq. (22) given below:

$$J_i = k_i(c_{s,i,max}-c_{s,i})^{\alpha_a}\,c_{s,i}^{\alpha_c}c_i^{\alpha_a}\left(exp\left(\frac{\alpha_aF}{RT}\eta_i\right) - exp\left(\frac{\alpha_cF}{RT}\eta_i\right)\right) \tag{22}$$

Here k_i is calculated using Eq. (23) and η is the surface over potential and can be calculated using the Eq. (24) below:

$$k_i = c_i(-10.5 + 0.668 \times 10^3 c_i + 0.494 \times 10^6 c_i^2 + 0.074T - 17.8c_iT - 8.86 \times 10^2 c_i^2 T - 6.96 \times 10^{-5} T^2 + 2.80 \times 10^{-2} c_i T^2) \quad (23)$$

$$\eta_i = \phi_{1,i} - \phi_{2,i} - U_i \quad (24)$$

Here ϕ_1 represents the potential in the solid phase, ϕ_2 represents the solution potential, and U represents the open circuit potential under the reference temperature. For this study, a single cell was simulated and the LIB model was considered isothermal at this scale. The energy balance for lithium-ion battery is given by

$$\rho C_p \frac{dT}{dt} = Q_{rxn} + Q_{rev} + Q_{ohm} \quad (25)$$

Here, Q_{rxn} is the total reaction heat generation rate, Q_{rev} is the reversible heat generation rate, and Q_{ohm} is the total ohmic heat generation rate. The total reversible heat generation rate is given by

$$Q_{rev} = FaJT \frac{\partial U}{\partial t} \quad (26)$$

The irreversible heat generation is the summation of Q_{rxn} total reaction heat generation and Q_{ohm} ohmic heat generation. The total reaction heat generation rate is given by

$$Q_{rxn} = FaJ\ (\phi_1 - \phi_2 - U) \quad (27)$$

The total ohmic heat generation rate is given by

$$Q_{ohm} = \sigma_{eff}\left(\frac{\partial \phi_1}{\partial x}\right)^2 + k_{eff}\left(\frac{\partial \phi_2}{\partial x}\right)^2 + \frac{2k_{eff}RT}{F}(1 - t_+^0)\frac{1}{C}\frac{\partial C}{\partial x}\frac{\partial \phi_2}{\partial x} \quad (28)$$

The temperature-dependent open circuit potential of electrode i is approximated by Taylor series first-order expansion around a reference temperature:

$$U_i = U_{i,ref} + (T - T_{ref})\left(\frac{dU}{dt}\right)_i \quad (29)$$

Here, $U_{i,ref}$ is the open circuit voltage (OCV) at a given reference temperature.

4 Results and Discussion

Using the parameters from Table 1 in COMSOL, the lithium-ion battery performance was analyzed. All the physical and geometrical parameters were obtained from previous literature [12,17,18]. The SOC-dependent OCV for NMC values were used from COMSOL built-in material properties. The model was then validated against the experimental results obtained by Stein et al. [12]. Figure 2 represents the graph of cell voltage versus capacity at 1 C discharge rate for experimental [12] and simulation results. The upper cutoff limit was set to be 4.2 V, and the lower cutoff limit was set to be 2.8 V. It can be seen that the maximum experimental capacity obtained is about 104.6 mAh/g. The simulation results maximum capacity matches that of the experimental results. There is a slight difference in the initial cell voltage of experimental and simulation results. This is because the COMSOL model used material properties to obtain OCV. However, the difference in the initial cell voltage is negligible. Experimental and simulation curves deviate from each other as the cell voltage decreases but after certain voltage both the curves overlap, each other till the battery's cutoff limit reaches 2.8 V. Overall, the model performed well in predicting the discharge behavior, which validates the COMSOL model.

Figure 3(*a*) shows the 1 C discharge, and 1 C and 5 C charge behavior for the thin electrode, and Fig. 3(*b*) shows 1 C discharge, and 1 C and 5 C charge behavior for the thick electrode. At 1 C the thin electrode delivers 104.6 mAh/g during discharge and can attain near that capacity during a 1 C charge. However, during a 5 C charge, the thin electrode achieves 24.9 mAh/g. For the thick electrode, 1 C discharge delivers 50.97 mAh/g. charging. This electrode at 1 C achieves 49.15 mAh/g while at 5 C only 11.36 mAh/g is recovered. The thin electrode has a shorter diffusion distance compared

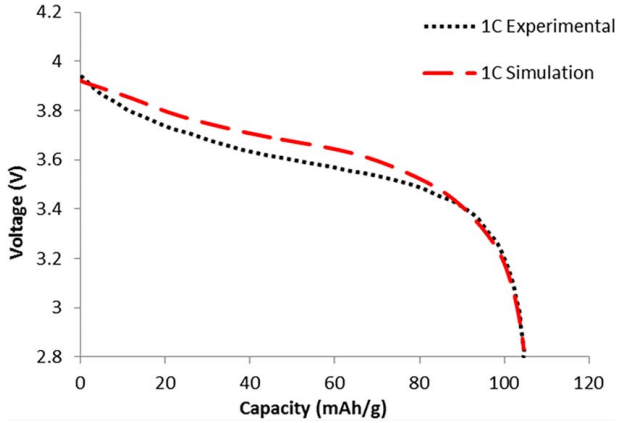

Fig. 2 Simulation discharge curve at 1 C compared to discharge behavior measured by Stein et al. [12]

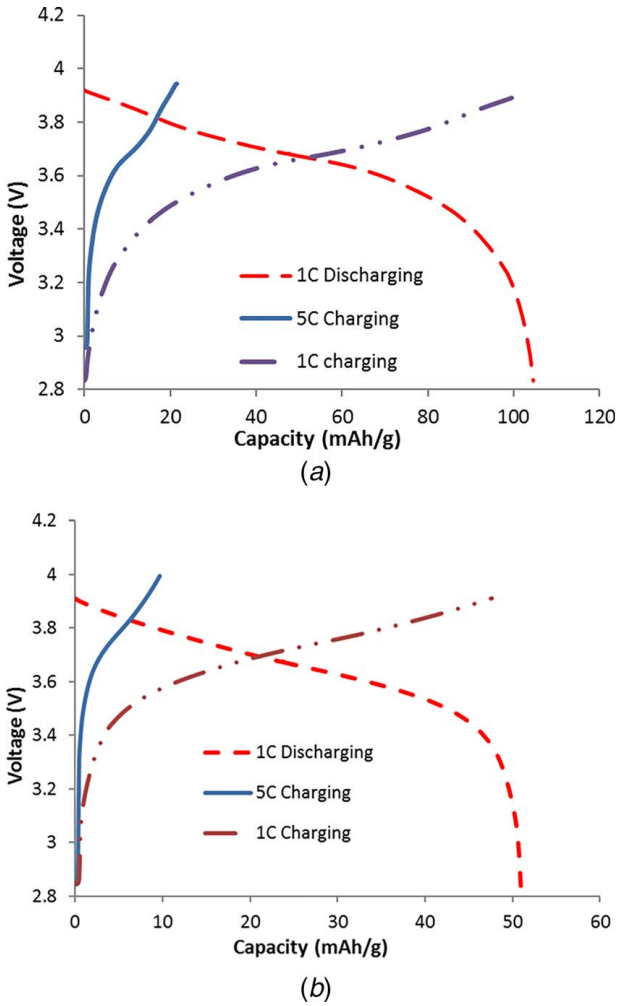

Fig. 3 (*a*) Discharge (1 C) and charge (1 C and 5 C) curves for thin electrode; (*b*) discharge (1 C) and charge (1 C and 5 C) curves for thick electrode

with the thick electrode so the internal resistance in the thick electrode is higher compared to the thin electrode. The thin and thick electrodes show similar trends for charge and discharge behaviors. However, for the thick electrode, the realized charge and discharge capacity is significantly lower compared with that of the thin electrode. Figure 3 shows that higher capacity is achieved in the thin electrode at lower C-rates compared with that in thick electrode. As C-rate and thickness of the electrode increases, the capacity achieved decreases. This is because at the higher C-rates, the lithium ion does not have enough diffusion time which makes it harder for Li-ion to fully access the entire active material region in the electrode and hence loses the cell capacity. Another aspect affecting the reduced realized capacity in the thick electrode is longer migration paths for lithium ions leaving or entering the electrodes. For the thicker electrode, the area near separator intercalates/deintercalates more lithium compared with the underlying regions. Considering this, the incoming lithium ions need to migrate longer distances to intercalate/deintercalate in the underlying regions of the electrode. The thinner electrode is therefore more dominated by kinetics and diffusion within the active material particle [20]. High charge–discharge rate shows less capacity due to the ohmic resistance as well as polarization effects, as indicated by the increased slope of the capacity curve. The discharge behavior of lithium-ion batteries is also affected by a change in particle size.

Figure 4 shows the cell voltage versus capacity graph of three different particle sizes for thin and thick electrodes. It can be seen that as the particle size increases the realized capacity decreases. This is because with the increasing particle size, the lithium-ion transport resistance increases and the full capacity of the active material particle becomes less accessible during a fixed charge or discharge time. This accessibility can be readily quantified based on a mass transfer Fourier number [20,21]. Also, the smaller particles have a more specific surface area, so the reaction rate is more rapid compared to the bigger particles. However, for thin electrodes, the change in the particle size does not show a significant change in capacity. In previous work, the particle size showed more dominance of short-range phenomena over long-range phenomena in the thin electrode [20]. For the thin electrode, kinetic overpotential influences more to charge and discharge behavior over particle size [20]. For the thick electrode, the change in particle size has a significant effect on capacity. While performing fast charge, the change in particle sizes shows no difference in capacity. This is because the cathode diffusion times for the particles sizes considered are either less than or comparable in magnitude to the discharge time of 720 s, and the thickness of the electrode presents the primary limitation on rate capability.

The change in porosity can also impact the realized capacity of the lithium-ion batteries. Figure 5 shows the cell voltage versus capacity graphs with varying porosity for thin and thick electrodes. The change in porosity does not significantly affect the capacity of the batteries with thin electrodes. In thin electrodes, the thickness of the electrode is small enough that the change in porosity does not

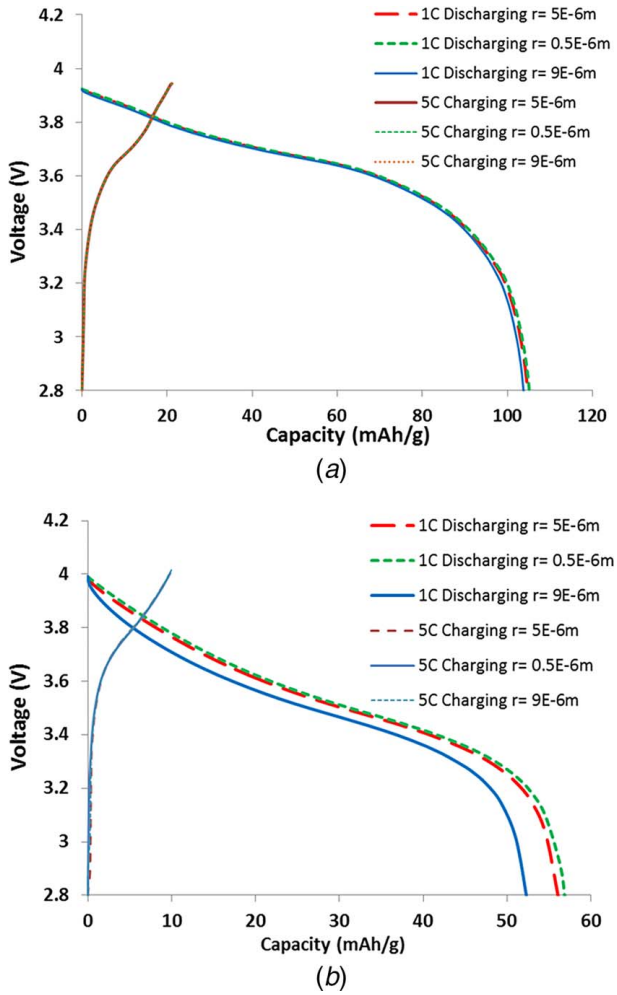

Fig. 4 (*a*) Discharge (1 C) curves with varying particle size for thin electrode; (*b*) discharge (1 C) curves with varying particle size for thick electrode

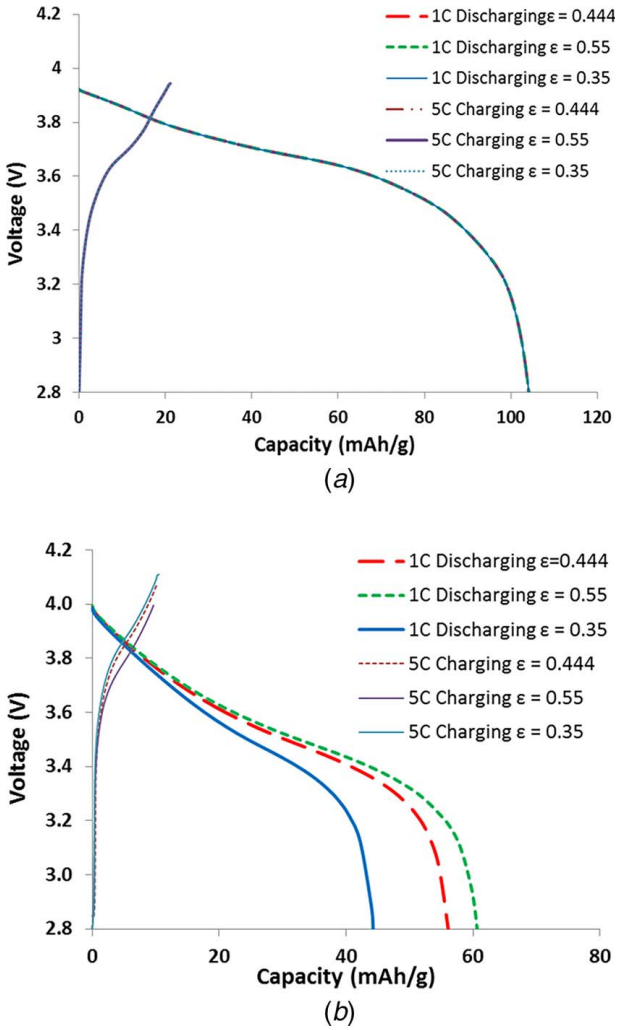

Fig. 5 (*a*) Discharge (1 C) and charging (5 C) curves with three different porosity values for thin electrode; (*b*) discharge (1 C) and charging (5 C) curves with three different porosity for thick electrode

show a large effect on lithium transport resistance, so the realized cell capacity does not change. While performing fast charging in the thin electrode, the change in porosity does not affect the capacity because all regions of the electrode can be reached effectively. However, for the thick electrodes, decreasing the porosity decreases the realized capacity. This is because decreasing porosity increases the lithium transport resistance, causing transport limitations in the electrolyte phase, which in turn affects access to the cell capacity. Decreasing the porosity of the electrode also increases the tortuosity of the electrode further hindering Li-ion transport, increasing internal resistance, and decreasing the realized cell capacity [22]. High internal resistance due to lower porosity can increase the ohmic heat generation in the cell. Lowering the porosity leads to mass transfer limitation and makes it difficult for Li ion in the electrolyte to access all potentially active surfaces in the electrode. The full capacity of the active material is not accessed, which lowers the realized cell capacity. In the thick electrode, the change in porosity also shows a variation in capacity while performing a fast charge. However, the change in capacity for thick electrode is not substantial. The primary variation is seen in the voltage achieved during fast charging, suggesting that the porosity impacts ohmic loss across the electrolyte phase in the battery. From Fig. 5(*b*), it can be seen that while performing 5 C charge, the cell with a thick electrode is overcharged. This increase in voltage while performing fast charge may indicate deposition lithium in excess of the original capacity of the electrode, highlighting the potential risk of lithium plating while performing fast charging.

How fast charge and gradual discharge affects the flow of lithium through the solid active material and lithium ions across the cell was analyzed. Figure 6 shows surface solid lithium concentration and electrolyte salt concentration for thin and thick electrode at 1 C and 5 C. The space between the profiles indicates the separator with a thickness of 26 μm. Profiles on the left side of this space are for the anode, and profiles on the right of this space are for the cathode. From Figs. 6(*a*) and 6(*c*), $t = 0$ s the anode is fully lithiated so the surface solid lithium concentration over the anode is higher compared to the cathode. As the discharge process begins the anode starts to delithiate and the cathode starts to lithate. At the end of 1 C discharge, i.e., $t = 3600$ s, the solid lithium concentration is higher on the cathode side compared to that on the anode. However, the interesting thing to note here is that the distribution of lithium concentration in the thicker electrode is uneven compared to the thinner electrode. This trend is the same while performing fast charging. This is because the thinner electrode does not have enough diffusion time and migration path for lithium ions is longer compared to the thin electrode. Considering that, the solid lithium concentration near the electrode/separator interface is higher compared to the underlying region of the electrode. This indicates the underutilization of the thicker electrode while performing a fast charge. Figures 6(*b*) and 6(*d*) show the electrolyte salt concentration for the thin and thick electrodes. Initially, at $t = 0$ s, the electrolyte salt concentration of the cell is 1000 mol/m^3. By the end of discharge, i.e., at $t =$?3600 s, it is observed that the variation in electrolyte salt concentration for a thin electrode is small compared to a thick electrode. This indicates small concentration polarization in thin electrode. While performing charging, as the C-rate and thickness of the electrode increase the concentration polarization and ohmic loss increases. This indicates a higher variation in electrolyte salt concentration in thin and thick electrodes, performing fast charge.

Figure 7 compares local current source for 1 C discharge and 5 C charge in batteries with thin and thick electrodes. During the 1 C discharge current enters the anode, which is represented by a positive sign in the graph, whereas current leaving the cathode is represented by a negative sign. This trend is reversed for the 5 C charging process. For thin and thick electrodes, during the 1 C discharge, the local current density is relatively uniform throughout the electrodes. However, while performing 5 C charging, the electrochemical reactions occur at a faster rate for both thin and thick electrodes. Transport within the electrode occurs at a slower rate relative to these

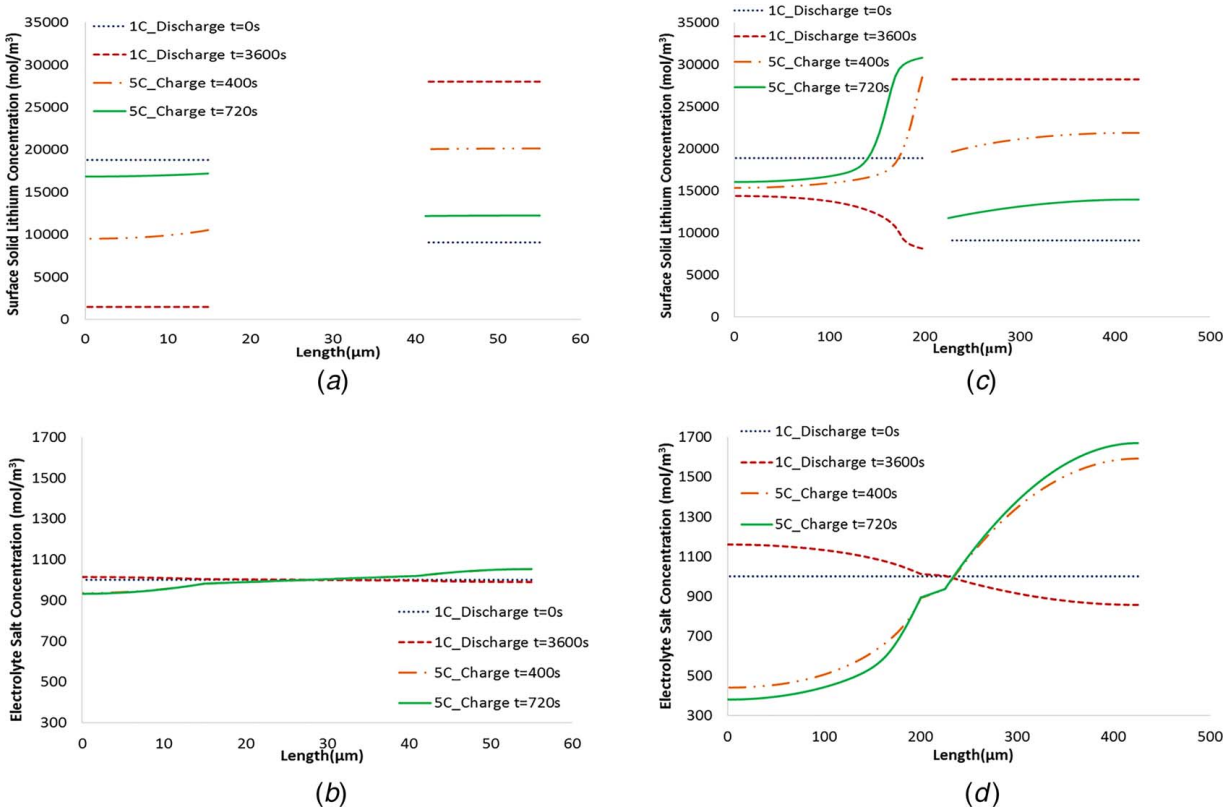

Fig. 6 (*a*) Surface solid lithium concentration for thin electrode, (*b*) electrolyte salt concentration for thin electrode, (c) surface solid lithium concentration for thick electrode, and (*d*) electrolyte salt concentration for thick electrode

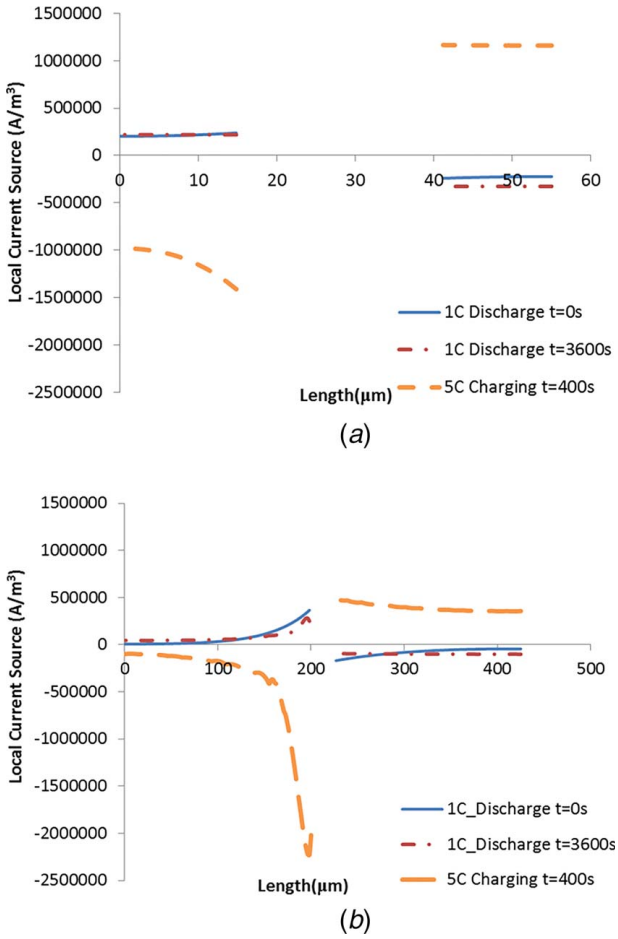

Fig. 7 (*a*) Local current source in thin electrode and (*b*) local current source in thick electrode

reactions. As a result, the local current density is distributed unevenly throughout the electrodes. This variation is more pronounced for thick electrodes where transport presents a greater limitation on the battery performance. While performing 5 C charge, local current density for thin and thick electrodes is high at the junction of electrode and separator. This is because at higher C-rates the electrochemical reaction at the electrode–separator junction becomes more rigorous which increases the flow of species near that region. The transport limitations noted above effectively focus on the reactions in this region of the battery.

While discharging and charging, the chemical reactions and internal resistance may give rise to heat generation. There are two types of heat generation considered, reversible heat generation and irreversible heat generation. Reversible heat is also called entropic heat, and it is a material property [23]. Irreversible heat is a combination of reaction and ohmic heating. Ohmic heating is due to electronic and ionic resistance from potential and concentration gradient. Reaction heating is due to the overpotential. There are various parameters affecting the heat generation in the cell. This section emphasizes how the thickness of the electrode affects the heat generation in the cell while accounting for particle size, porosity, C-rate, and electrode thickness. Cases analyzed are based primarily on the active material particle size in the anode and cathode, with four cases outlined in Table 2. Figures 8 and 9 show reversible and irreversible heat generation, respectively, at the beginning of the 1 C discharge, at the end of the 1 C discharge, and at 400 s into the 5 C charging both thin and thick electrodes. Figure 10 presents total heat generation which is dependent on reversible and irreversible heat sources. As the thickness of the electrode increases internal resistance increases which increases the heat generation in the battery.

Table 2 Active material particle size combinations for heat generation assessment

Case	Anode particle size (μm)	Cathode particle size (μm)
1	5	5
2	5	0.5
3	0.5	5
4	0.5	0.5

It can be seen from Figs. 8 and 9 that thicker electrode produces more heat compared to the thinner electrode. At $t = 0$ s when electrochemical reactions are initiating the reversible and irreversible heat generation is less, so the total heat generation is less. At $t = 3600$ s, the total heat generation is higher compared to the beginning of the 1 C discharge. From Fig. 8 initially the reversible heat source is negative for the anode. This is because reversible heat generation is a material property, and graphite has a strong entropic response leading to a negative reversible heat generation [24]. Hence, the anode is dominating when it comes to reversible heat generation. While performing aggressive 5 C charging, the electrochemical reactions become more rigorous and local current density is elevated (Fig. 7). Combined with the internal resistance, this leads to an increased heat generation compared with slower discharge or charge. In Figs. 8 and 9, it can be seen that at $t = 400$ s for the 5 C charging the heat generated is higher compared to 1 C discharging.

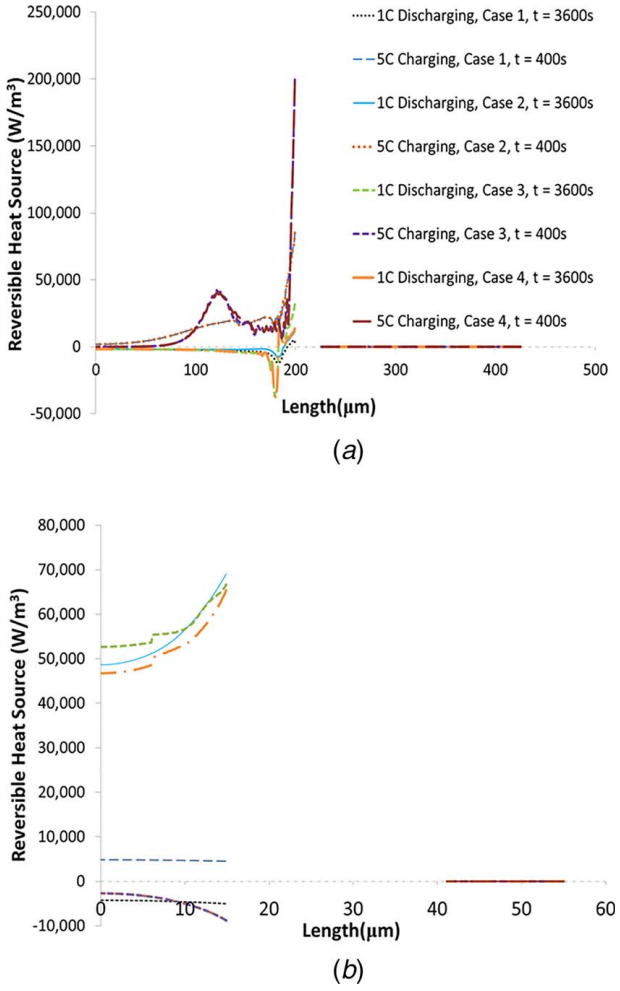

Fig. 8 (*a*) Reversible in a thick electrode and (*b*) reversible heat generation in a thin electrode during 1 C discharge and 5 C charge for distinct combinations of particle sizes. Legend shown in (*a*) applies to both plots

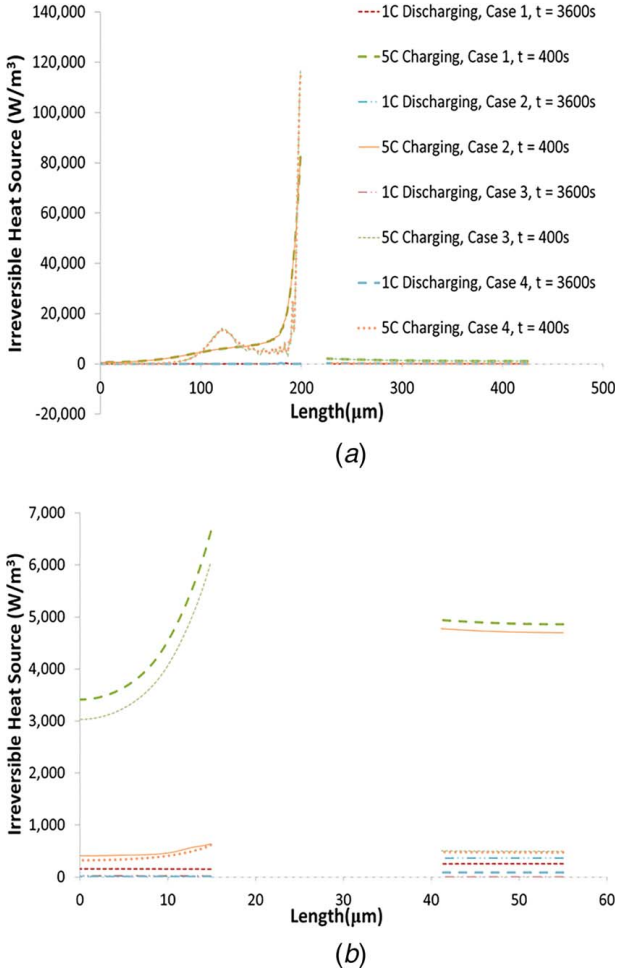

Fig. 9 (*a*) Irreversible heat generation in a thick electrode and (*b*) irreversible heat generation in a thin electrode during 1 C discharge and 5 C charge for distinct combinations of particle sizes. Legend shown in (*a*) applies to both plots

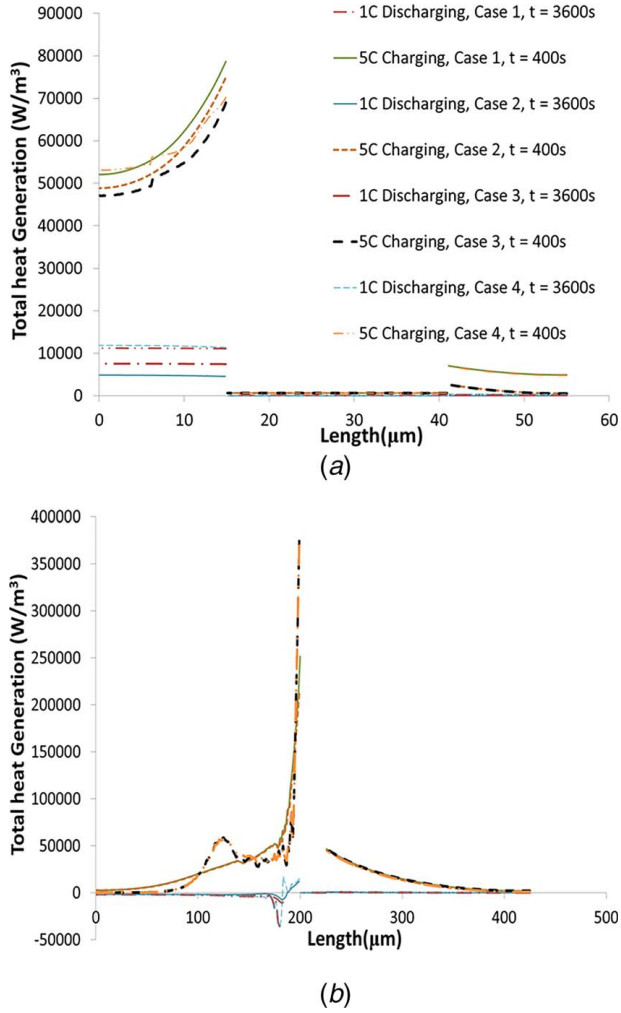

Fig. 10 (*a*) Total heat generation in a thin electrode during 1 C discharge and 5 C charge compared with (*b*) total heat generation in a thick electrode for distinct combinations of particle sizes

The maximum ohmic heat generation in cell occurs at the electrode–separator interface. This is due to the higher potential and concentration gradients of the species near the electrode–separator junction than other areas. The interesting thing to note here is that the distribution of heat generated is uneven throughout the electrodes. This local increase is due to the non-uniform current brought about by the transport limitations within the electrode. Transport limitations within the cell focus on the electrochemical reactions at this interface and lead to high local heating. This uneven distribution can lead to faster aging of active material near the separator compared to the active material present at the current collector edge of the electrode.

5 Conclusion

In this work, a pseudo-2D model of lithium-ion battery operation was created using COMSOL MULTIPHYSICS 5.2 software. The motivation behind this work was to understand how various parameters like porosity, active material particle size, and electrode thickness affect the charge and discharge behavior. The emphasis was placed on the assessment of local field variables and key responses like local current and heat generation within a single-cell stack. Based on simulation results obtained, as the thickness of the electrode increases the realized capacity decreases. For thick electrodes, a change in active material particle size showed a significant effect on discharge behavior compared with thin electrode. As the particle size increases, the realized capacity decreases for the given electrode. Changes in porosity had no significant effect on the discharge behavior in thin electrodes. However, increasing porosity in thick electrodes increased the realized battery capacity. While performing 1 C discharge, the heat generation in thin electrodes was evenly distributed whereas heat generation in thick electrodes was unevenly distributed throughout the electrode. As the C-rate increases, the uneven nature of the heat generation in thick electrodes becomes more pronounced compared with thin electrodes. The important factors behind higher heat generation in thick electrodes are lithium transport limitations, which increase internal resistances, and more rigorous electrochemical reactions, which increase local current densities. Increasing the discharge rate increases the heat generation in the battery which can eventually deteriorate the health of lithium-ion battery. Higher heat generation in the battery can lead to fast aging of the active material which can further reduce the capacity of the battery over its life cycle.

Acknowledgment

Financial support from an NSF CAREER Award (CBET-1454437) is gratefully acknowledged.

References

[1] Lu, L., Han, X., Li, J., Hua, J., and Ouyang, M., 2013, "A Review on the Key Issues for Lithium-Ion Battery Management in Electric Vehicles," J. Power Sources, **226**, pp. 272–288.

[2] Wagner, R., Preschitschek, N., Passerini, S., Leker, J., and Winter, M., 2013, "Current Research Trends and Prospects Among the Various Materials and Designs Used in Lithium-Based Batteries," J. Appl. Electrochem., **43**(5), pp. 481–496.
[3] Whittingham, M. S., 2004, "Lithium Batteries and Cathode Materials," Chem. Rev., **104**(10), pp. 4271–4302.
[4] Ellis, B. L., Lee, K. T., and Nazar, L. F., 2010, "Positive Electrode Materials for Li-Ion and Li-Batteries," Chem. Mater., **22**(3), pp. 691–714.
[5] Tarascon, J. M., and Armand, M., 2001, "Issues and Challenges Facing Rechargeable Lithium Batteries," Nature, **414**(6861), pp. 359–367.
[6] Singh, M., Kaiser, J., and Hahn, H., 2015, "Thick Electrodes for High Energy Lithium Ion Batteries," J. Electrochem. Soc., **162**(7), pp. A1196–A1201.
[7] Zhao, R., Liu, J., and Gu, J., 2015, "The Effects of Electrode Thickness on the Electrochemical and Thermal Characteristics of Lithium ion Battery," Appl. Energy, **139**, pp. 220–229.
[8] Ecker, M., Sabet, P. S., and Sauer, D. U., 2017, "Influence of Operational Condition on Lithium Plating for Commercial Lithium-Ion Batteries—Electrochemical Experiments and Post-Mortem-Analysis," Appl. Energy, **206**, pp. 934–946.
[9] Zinth, V., Lüders, C. V., Hofmann, M., Hattendorff, J., Buchberger, I., Erhard, S., Rebelo-Kornmeier, J., Jossen, A., and Gilles, R., 2014, "Lithium Plating in Lithium-Ion Batteries at Sub-Ambient Temperatures Investigated by In Situ Neutron Diffraction," J. Power Sources, **271**, pp. 152–159.
[10] Mistry, A., Juarez-Robles, D., Stein, M., Smith, K., and Mukherjee, P. P., 2016, "Analysis of Long-Range Interaction in Lithium-Ion Battery Electrodes," ASME J. Electrochem. Energy Convers. Storage, **13**(3), p. 031006.
[11] Taleghani, S. T., Marcos, B., Zaghib, K., and Lantagne, G., 2017, "A Study on the Effect of Porosity and Particles Size Distribution on Li-Ion Battery Performance," J. Electrochem. Soc., **164**(11), pp. E3179–E3189.
[12] Stein, M., Chen, C., Mullings, M., Jaime, D., Zaleski, A., Mukherjee, P. P. and Rhodes, C. P. 2016, "Probing the Effect of High Energy Ball Milling on the Structure and Properties of LiNi1/3Mn1/3Co1/3O2 Cathodes for Li-Ion Batteries," ASME. J. Electrochem. Energy Convers. Storage, **13**(3), p. 031001.
[13] Tran, T. D., Feikert, J. H., Pekala, R. W., and Kinoshita, K., 1996, "Rate Effect on Lithium-Ion Graphite Electrode Performance," J. Appl. Electrochem, **26**(11), pp. 1161–1167.
[14] Bandhauer, T. M., Garimella, S., and Fuller, T. F., 2011, "A Critical Review of Thermal Issues in Lithium-Ion Batteries," J. Electrochem. Soc., **158**(3), p. R1.
[15] Thomas, E. V., Case, H. L., Doughty, D. H., Jungst, R. G., Nagasubramanian, G., and Roth, E. P., 2003, "Accelerated Power Degradation of Li-Ion Cells," J. Power Sources, **124**(1), pp. 254–260.
[16] Bae, C.-J., Erdonmez, C. K., Halloran, J. W., and Chiang, Y.-M., 2012, "Design of Battery Electrodes With Dual-Scale Porosity to Minimize Tortuosity and Maximize Performance," Adv. Mater., **25**(9), pp. 1254–1258.
[17] Doyle, M., 1993, "Modeling of Galvanostatic Charge and Discharge of the Lithium/Polymer/Insertion Cell," J. Electrochem. Soc., **140**(6), p. 1526.
[18] Guo, M., Kim, G. H., and White, R. E., 2013, "A Three-Dimensional Multi-Physics Model for a Li-Ion Battery," J. Power Sources, **240**, pp. 80–94.
[19] Gu, W. B., and Wang, C. Y., "Thermal-Electrochemical Coupled Modeling of a Lithium-Ion Cell," J Electrochem Soc, **99**(8), pp. 748–762
[20] Rajendra, T., Mistry, A. N., Patel, P., Ausderau, L. J., Xiao, X., Mukherjee, P. P., and Nelson, G. J., Aug. 2019, "Quantifying Transport, Geometrical, and Morphological Parameters in Li-Ion Cathode Phases Using X-ray Microtomography," ACS Appl. Mater. Interfaces, **11**(22), pp. 19933–19942.
[21] Nelson, G. J., Ausderau, L. J., Shin, S., Buckley, J. R., Mistry, A., Mukherjee, P. P., and De Andrade, V., 2017, "Transport-Geometry Interactions in Li-Ion Cathode Materials Imaged Using X-Ray Nanotomography," J. Electrochem. Soc., **164**(7), pp. A1412–A1424.
[22] Chen, C.-F., Verma, A., and Mukherjee, P. P., 2017, "Probing the Role of Electrode Microstructure in the Lithium-Ion Battery Thermal Behavior," J. Electrochem. Soc., **164**(11), pp. E3146–E3158.
[23] Thomas, K. E., and Newman, J., 2003, "Heats of Mixing and of Entropy in Porous Insertion Electrodes," J. Power Sources, **119–121**, pp. 844–849.
[24] Gröger, O., Gasteiger, H. A., and Suchsland, J.-P., 2015, "Review Electromobility: Batteries or Fuel Cells?," J. Electrochem. Soc., **162**(14), pp. A2605–A2622.